energies

MDPI

Article

Performance Assessment of Two Different Phase Change Materials for Thermal Energy Storage in Building Envelopes

Ruta Vanaga *, Jānis Narbuts, Ritvars Freimanis, Zigmārs Zundāns and Andra Blumberga

Institute of Energy Systems and Environment, Riga Technical University, 1048 Riga, Latvia; janis.narbuts_1@rtu.lv (J.N.)

* Correspondence: ruta.vanaga@rtu.lv

Abstract: To meet the 2050 EU decarbonization goals, there is a need for new and innovative ideas to increase energy efficiency, which includes reducing the energy consumption of buildings and increasing the use of on-site renewable energy sources. One possible solution for achieving efficient thermal energy transition in the building sector is to assign new functionalities to the building envelope. The building envelope can function as a thermal energy storage system, which can help compensate for irregularities in solar energy availability. This can be accomplished by utilizing phase change materials as the energy storage medium in the building envelope. In this paper, two phase change materials with different melting temperatures of 21 °C and 28 °C are compared for their application in a dynamic solar building envelope. Both experimental and numerical studies were conducted within the scope of this study. The laboratory testing involved simulating the conditions of the four seasons through steady-state and dynamic experiments. The performance of the phase change materials was evaluated using a small-scale PASLINK test stand that imitates indoor and outdoor conditions. A numerical model of a small-scale building envelope was created using data from laboratory tests. The purpose of this model was to investigate how the tested phase change materials perform under different climate conditions. The experimental findings show that RT21HC is better at storing thermal energy in the PCM and releasing it into the indoor area than RT28HC. On the other hand, the numerical simulation results demonstrate that RT28HC has an advantage in terms of thermal storage capacity in climates found in Southern Europe, as it prevents overheating of the room.

Keywords: building envelope; solar thermal energy storage; melting temperature; latent heat; small-scale PASLINK test; ANSYS Fluent

Citation: Vanaga, R.; Narbuts, J.; Freimanis, R.; Zundāns, Z.; Blumberga, A. Performance Assessment of Two Different Phase Change Materials for Thermal Energy Storage in Building Envelopes. *Energies* **2023**, *16*, 5236. https://doi.org/10.3390/en16135236

Academic Editor: Francesco Minichiello

Received: 31 March 2023
Revised: 24 April 2023
Accepted: 16 May 2023
Published: 7 July 2023

1. Introduction

The EU Green Deal aims to achieve a decarbonized building stock by 2050 and advocates for the utilization of renewable energy sources (RES) and intelligent technologies in buildings to attain this goal [1–3]. The definition of nearly zero-energy buildings is proposed as one of the approaches towards decarbonizing building stock, which recommends the usage of on-site available renewable energy sources to meet the energy requirements. However, there are inconsistencies between the availability of renewable technologies and the energy demand, unlike the case of conventional fossil energy. Renewable energy technologies may exceed the demand during peak periods or may not be sufficient to meet the energy needs during low periods, and they exhibit diurnal and seasonal fluctuations depending on the type of renewable energy technology employed. Each member state in the EU defines the benchmark for cost-effective nearly zero-energy buildings. Lowering the benchmark for heating energy demand in the northern climate is more challenging. Innovative concepts for building thermal envelopes might provide a breakthrough in the energy transition. Converting the thermal envelope of a building into a solar thermal energy storage unit is one promising path that would increase the share of on-site renewables

in covering the heating and cooling energy demand. In recent years, the acceptance of phase change materials (PCM) in building envelopes has increased due to their thermal energy transition characteristics. Ahangari and Maerefat performed a numerical study comparing the performance of a facade system consisting of concrete, insulation, and soil/plaster layers with the same façade system enhanced by two layers of PCM with different melting temperatures. The simulation results indicated that applying a double PCM layer reduced energy consumption for heating in dry and semi-arid climates in the amounts of 17.5% and 10.4%, respectively [4]. In another study, Saffari researched the improvement of energy flexibility in buildings by using PCM-enhanced envelopes. The results show that the maximum energy flexibility efficiencies range from 250% for the LW Gypsum Board envelope to 356% for the LW PCM-2 envelope [5]. PCM building envelopes can also be used to reduce the load from cooling systems in hot environmental conditions. Referring to Alshuraiaan, the thermal energy flow to indoor space can be reduced by 50% by using a PCM with a suitable melting temperature in the building envelope [6]. A detailed literature review of PCM building envelopes used in various climates has been conducted by Arumugam [7], with the conclusion that buildings with integrated PCM elements have significantly reduced energy demands. Moreover, it is stated that to improve building energy performance in warmer climate zones, PCM elements should be integrated into the outer surface of the wall, while, on the contrary, for colder climate zones they should be built into the innermost layer of the building envelope. Most of the techniques where PCM elements are used in building envelopes are passive and they perform most successfully only in steady climate zones where temperature changes are gradual. To achieve better energy performance and improve the energy efficiency of the whole building throughout the whole year in climate zones with different seasons and constantly changing weather, it is necessary to equip homes with building envelopes that can interact with irregular ambient environment changes and available on-site renewable energy sources, such as solar power.

1.1. Goal and Scope of the Study

The authors of this study are working on developing an innovative and adaptive dynamic solar building envelope that can be utilized in various locations worldwide, regardless of the climate zone. In this paper, comparative research is performed with PCMs that have two different melting point temperatures. The aim of this study was to identify the most appropriate PCM melting temperature for use in a dynamic solar facade module with thermal energy storage, which will be integrated into a large-scale adaptive dynamic solar facade system. The selected PCM should be suitable for application in various climate zones. Choosing the most appropriate PCM, and knowledge of the PCM behavior under different climatic loads is vital in the scope of this study as well as for other scientific or industrial research projects using PCM-enhanced building envelopes. Laboratory experiments were conducted under controlled temperature and solar radiation conditions to determine the PCM that is most appropriate for a specific application. Additionally, a numerical model was created to investigate the viability of this technology in varying climate zones. The main indicator is the exhibition of latent heat energy storage and its impact on indoor temperature dynamics. A testing setup to compare the thermodynamic processes in the selected PCMs was created in the laboratory at Riga Technical University Institute of Energy Systems and Environment.

1.2. Literature Review of PCM Numerical Modeling

The primary objective of numerical modeling is to replicate laboratory conditions that mimic real-life scenarios in various climate zones, where there are changes in temperature and solar irradiation. This can aid in assessing the performance of a PCM under different environmental conditions. ANSYS Fluent is among the most used software to model PCM-enhanced building envelopes [8]. A more in-depth investigation of ANSYS-based modeling of PCM-enhanced building envelopes was conducted. To perform a bibliometric

analysis, the researchers utilized the Web of Science (WOS) online database and selected publications based on keywords such as "building", "PCM", "phase change material", "paraffin", "simulation", "numerical analysis", "model", "software", and "ANSYS". To refine the scope of the search, the publications were filtered based on their document types, which included articles, early access, and review articles. The search was limited to the years 2019–2023. The analysis yielded 42 publications, of which seven were irrelevant to the search scope and thus excluded from further examination. Out of all the studies chosen, only nine met the two main requirements: utilizing ANSYS Fluent simulation software and focusing on walls as the object of research. The publications meeting these criteria are detailed in Table 1.

Table 1. WOS selection of publications on ANSYS modeling of PCM-enhanced building components.

Publication	Time Scale	Scale (Element, Room, or Building)	Building Envelope
Performance Evaluation of an Active PCM Thermal Energy Storage System for Space Cooling in Residential Buildings [9]	Month	Room	Wall
Comparative Study of Two Materials Combining a Standard Building Material with a PCM [10]	Hour	Element	Wall
Numerical Simulation of a Novel Dual Layered Phase Change Material Brick Wall for Human Comfort in Hot and Cold Climatic Conditions [11]	Month	Element	Wall
Parametric analysis and design optimisation of PCM thermal energy storage system for space cooling of buildings [12]	Day	Room	Wall
Thermal management analysis of PCM integration in building using a novel performance parameter—PCM effectiveness index [13]	Year	Room	Wall, roof
Numerical analysis of nanomaterial-based sustainable latent heat thermal energy storage system by improving thermal characteristics of phase change material [14]	Seconds	Element	Wall, floor
Simulation of a Trombe wall with a number of semicircular fins placed on the absorber plate for heating a room in the presence of nano-PCM [15]	Hour	Room	Wall
Numerical thermal evaluation of laminated binary microencapsulated phase change material drywall systems [16]	Month	Room	Wall
Potential of integrating PCMs in residential building envelope to reduce cooling energy consumption [17]	Hour	Room	Wall

1.3. Thermal Energy Storage

The ability to store thermal energy is crucial in renewable energy systems as it allows for better management of energy demand and increases flexibility. Thermal energy storage can be divided into two main categories: thermal storage (which includes sensible and latent storage) and thermochemical energy storage (as shown in Figure 1). Currently, sensible heat storage is widely available commercially (accumulation tanks in heating systems), while others are still under development [18,19]. Sensible heat storage depends on the mass and heat capacity of the material, while latent energy storage is calculated in two states, before phase change and after the phase change (as a sensible heat), and, in addition, the enthalpy of fusion (J/g) is taken into account. There are three types of thermal energy storage systems, based on sensible, latent, and thermochemical heat storage, but the first two are more applicable in buildings. Sensible heat storage systems are simpler and already available on the market, whereas latent heat thermal energy storage systems

(LHTES) have a higher storage capacity per unit volume [20]. Such systems are applicable and convenient for passive and net-zero energy buildings as they can be directly implanted into building envelopes that use on-site renewable energy sources, namely solar thermal energy. The most important advantage of the application of correspondent technology is the reduction in heating season duration, especially in climate zones where the autumn and spring seasons are long.

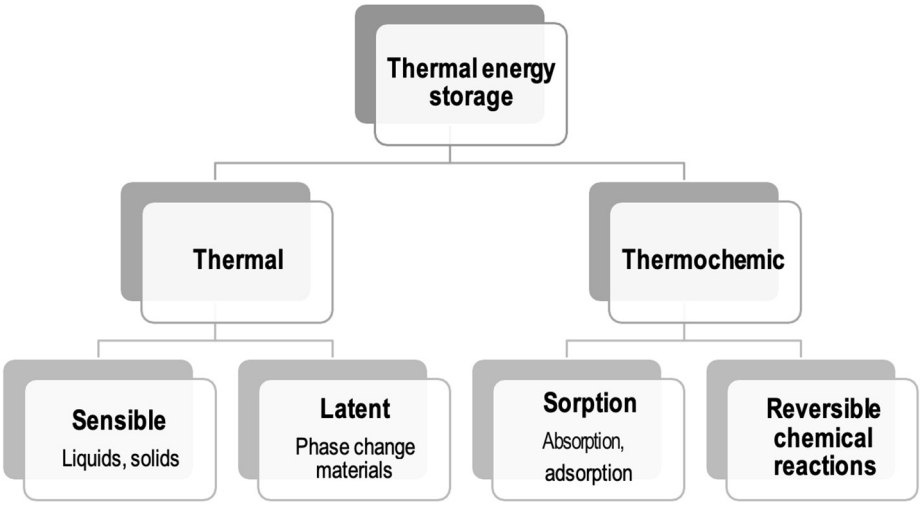

Figure 1. Classification of thermal energy storage methods.

Thermal energy storage techniques vary in terms of their operating temperature range, storage capacity, and duration of storage, which can range from hours to months for seasonal storage. These methods are used to balance energy demand between day and night, store summer heat for winter heating, and store winter cold air for summer air conditioning. Among the thermal energy storage methods, sensible heat storage is the most versatile, covering the widest range of operating temperatures (sub-zero to 500 °C) and can be utilized on both an hourly and seasonal scale [21]. Yet for application in building thermal envelopes the most suitable temperature range is 18–50 °C (given for different types of paraffin wax) [22]. Storing thermal energy for later use through heating or cooling an energy storage medium is known as thermal energy storage (TES). These systems can help balance the fluctuations in the availability of renewable energy sources (RES) on a daily or seasonal basis. In PCMs, energy can be stored as either sensible or latent heat [23]. Sensible heat is the measure of energy necessary to change a body's temperature, whereas latent heat occurs at a nearly linear temperature while changing the phase of the substance (solid to liquid, liquid to gaseous, solid to solid) [24] (see Figure 2).

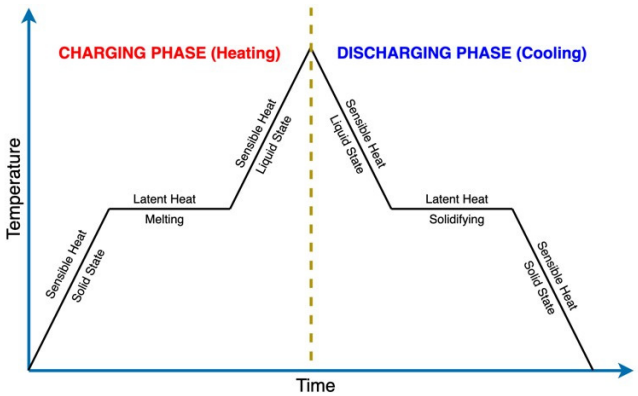

Figure 2. Theoretical latent heat curve for solid/liquid phase transition.

In the charging phase, the heat is applied to the PCM and the energy is stored, while in the discharging phase, the stored heat is released. Incorporating TES into an energy system provides several benefits, such as improved performance and reliability, better economics, reduced maintenance and operating costs, and decreased environmental pollution. This includes lower carbon dioxide emissions as the energy demand for heating decreases [18]. Both passive and active techniques are utilized for TES in a range of settings, including HVAC systems, building structures, and systems located near buildings [25].

1.4. Phase Change Materials

PCM is utilized as the energy storage medium in LHTES systems (see Figure 3).

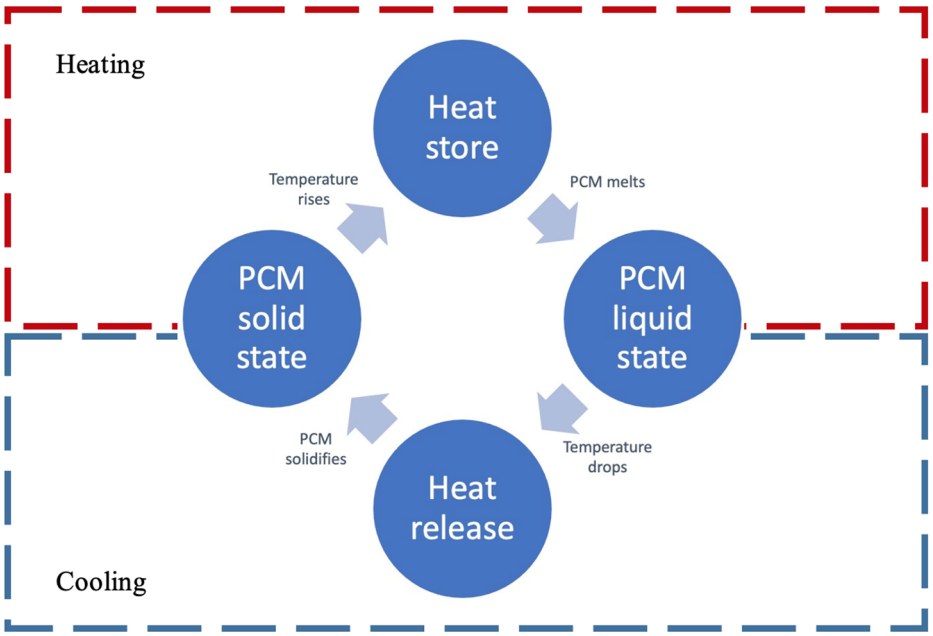

Figure 3. The working cycle of phase change material.

In building applications, solid–liquid PCMs are commonly used and are classified into three main categories: organic, inorganic, and eutectics [26]. Paraffin, fatty acid, and sugar alcohols are the most commonly used organic PCMs, with paraffin having the advantage of a phase change temperature range from 10 °C to 100 °C [27]. Various studies have been conducted on incorporating phase change materials into building components such as boards, bricks, and shading devices [28–30]. Despite this, PCM-enhanced building components have not yet reached the mass production level, leaving room for potential optimization and innovation. Scientific understanding of PCM behavior and characteristics can pave the way for technological advancements. The melting temperature of a PCM is one of the parameters that determine its suitability for specific building applications with defined performance objectives, such as reducing heating or cooling loads, and the environment in which the PCM-enhanced building component is placed, including daily and seasonal temperature ranges.

2. Materials and Methods

2.1. Materials

The design of the test stands incorporates various materials, including extruded polystyrene (XPS) from Finfoam (Salo, Finland) for insulation, plywood from Ergos (Riga, Latvia) for external construction, glass from Glass (Riga, Latvia) for containers, polyethylene terephthalate glycol (PETG) from Prusa Research (Prague, Czech Republic) for container covers, and PCMs from Rubitherm Technologies GmbH (Berlin, Germany) for experimental study. These RTHC PCMs are composed of organic materials, such as paraffin wax, which

undergo a solid-to-liquid (and vice versa) melting process to efficiently store and release substantial amounts of heat within a relatively constant temperature range [31]. These versatile PCMs can be used in a wide range of applications at various temperatures, depending on their melting point. One notable advantage of RTHC PCMs is their significantly higher latent heat capacity of 25–30% compared to traditional PCMs, and they melt within a narrower temperature range. This makes them well-suited for situations where space is limited, as they are ideal for efficient thermal energy storage in confined spaces. The properties and characteristics of the materials used in the design of the test stands are summarized in Table 2.

Table 2. Material properties and characteristics.

Material	Properties	Characteristics
RUBITHERM RT21HC	Dimensions: 127 × 127 × 60 mm^3	Melting area: 20–23 °C Congealing area: 21–19 °C Density at 15 °C: 0.88 kg/L Density at 40 °C: 0.77 kg/L Heat storage capacity ±7.5% 190 kJ/kg
RUBITHERM RT28HC	Dimensions: 127 × 127 × 60 mm^3	Melting area: 27–29 °C Congealing area: 29–27 °C Density at 15 °C: 0.88 kg/L Density at 40 °C: 0.77 kg/L Heat storage capacity ±7.5% 250 kJ/kg
Plywood	Thickness: 15 mm	λ = 0.13 W/mK SHGC = 0.28
XPS	Thickness: 50 mm	λ = 0.037 W/mK
Glass	Thickness: 4 mm	λ = 1.2 W/mK SHGC = 0.8
PETG	Thickness: 2 mm	λ = 0.2 W/mK

2.2. PASLINK-Type Testing

To evaluate the performance of each of the PCMs, comparative testing was performed based on the PASLINK testing method. This method is one of the most commonly used methods for testing passive solar-thermal-energy-based building components and envelopes. PASLINK evolved from the European project PASSYS (Testing Passive Solar Energy Components and Systems), which began in 1985 with the aim of increasing confidence in both the use of energy-efficient and passive solar buildings and their assessment methods [32]. The PASSYS project focused on a test cell bench as a means of determining the energy performance of passive solar building components and providing more information on building design and simulation tools [33]. The advantage of test cells is that they provide a well-controlled environment [34].

2.3. Experimental Setup

The thermal energy transmission rate of the dynamic solar building envelope is largely influenced by the various components that make up its overall design. Figure 4 shows an innovative design of a building envelope developed by the research team. The design incorporates a PCM container, an aerogel layer to minimize heat loss, and a heat transfer enhancer (Fresnel lens), which concentrates solar energy onto the surface of the PCM container. This study focuses on the use of latent heat thermal energy storage, where a PCM is the main component responsible for thermal energy transfer through the building envelope. Choosing the optimal PCM can significantly reduce heating and cooling loads, particularly during periods when solar radiation is available. Various factors must be

considered when selecting the PCM for specific applications, including the optimal volume, layer thickness, and melting temperature range, as outlined by Guo and Zhang [35].

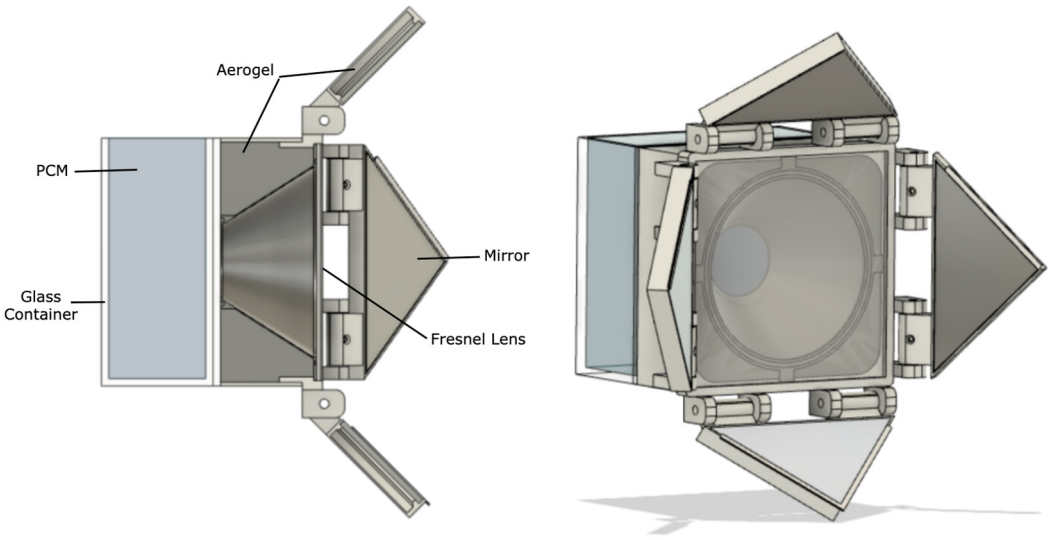

Figure 4. The design of a solar building envelope module.

The optimal PCM volume and layer thickness must be selected to ensure geometric compatibility with other components of the system, including the Fresnel lens focal length and point location, aerogel insulation layer, and dimensions of the large-scale system (an upscaled version of the small-scale module). The system aims to provide an efficient energy balance for the entire building while maintaining a comfortable indoor environment for occupants, with room temperatures ranging from 18 °C to 27 °C throughout all seasons.

To compare the thermal behavior of two different PCMs under different climatic conditions simulating different seasons of the year, two comparative experiments—steady-state and dynamic—were conducted in laboratory testing. While Rubitherm RT21HC has a lower melting temperature closer to the average indoor temperature, Rubitherm RT28HC has a higher latent heat storage capacity. The experimental setup was designed to replicate a small-scale PASLINK-type test cell, with two test stands prepared for the comparative study—one for RT21HC and the other for RT28HC. The plywood box was lined with 50 mm insulation (XPS) to simulate the "indoor" space, and the PCM container was built into one of the walls of each test box (see Figure 5).

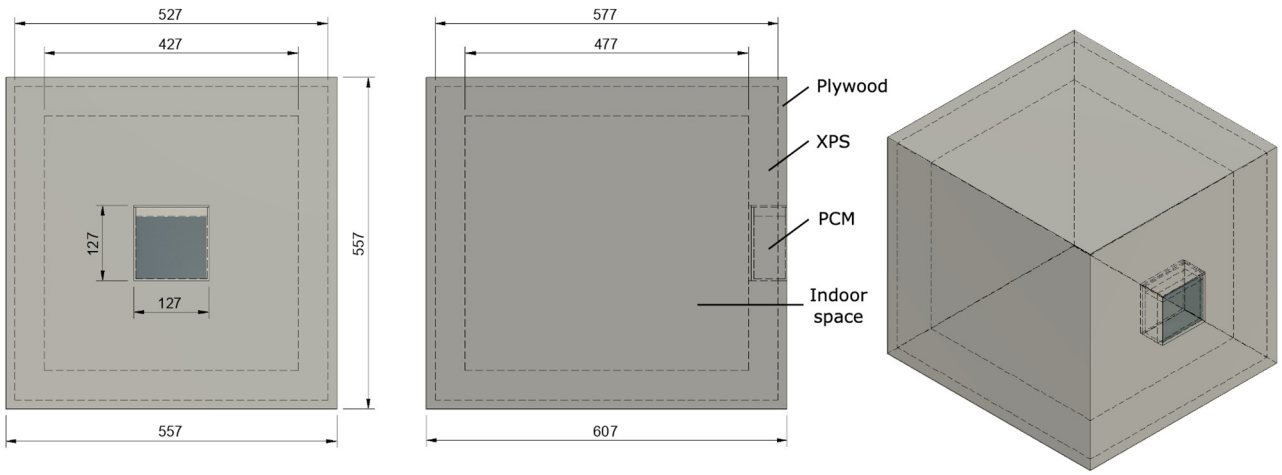

Figure 5. Test box. Small-scale PASSLINK-type test cell.

To monitor the experimental setup, a set of thermocouples was placed as shown in Figure 6. A total of eleven thermocouples were installed for each test box—six placed in the PCM container at different heights to observe temperature changes in different layers of the phase change materials and five thermocouples located in the indoor space of the test box at different heights. The thermocouples are labeled based on their location inside the PCM container, with letters L, M, and R indicating their location on the x-axis (L—left, M—middle, and R—right), and numbers indicating their location on the y-axis (1—lower and 2—upper). This set of thermocouples allows for a comparison of changes in PCM temperature and indoor space temperature between the two setups under defined conditions. The test stands were positioned adjacent to each other inside the climatic test chamber Tera Science TEMI 2500 (Changwon, Republic of Korea), as illustrated in Figure 7.

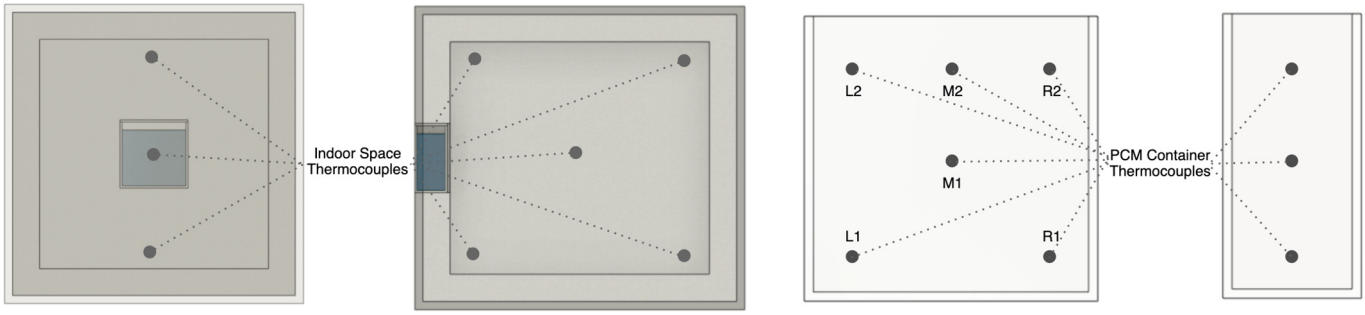

Figure 6. Thermocouples in small-scale PASLINK-type testing boxes (**left**) and PCM container (**right**).

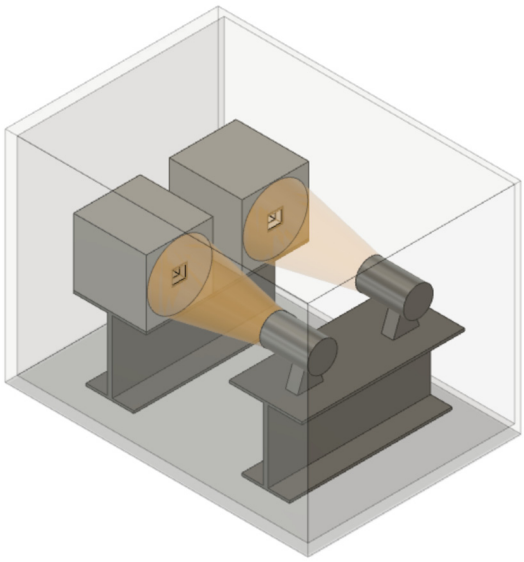

Figure 7. Experimental setup in the climate chamber.

Solar energy consists of radiant light and heat from the Sun [36]. To simulate solar radiation for the test setups, halogen lamps were used since they emit both heat and light with color characteristics similar to that of the Sun [37]. Specifically, two halogen lamps (GE SUPER CP60 EXC VNS 230V | 1000W G16d 3200K | General Electric (Schenectady, NY, USA) combined with dimmer UNI BAR Elation professional) were positioned along the longitudinal axes of each test box. A heating/cooling unit was utilized to maintain the desired temperature within the climatic chamber. The experimental setup is designed as a miniature version of a "structure", comprising a test box with a thermal enclosure and indoor area. This setup is exposed to climate-induced stresses such as heating and cooling, which are created by the predetermined conditions in the climate chamber. Temperature changes in both the indoor space and the phase change material of the thermal enclosure are recorded using measuring equipment.

2.4. Planning of the Experiment

The test conditions were designed to simulate the four seasons: spring, summer, autumn, and winter. For the steady-state experiment, three identical 24 h cycles were repeated for each season. The conditions for each season are determined by the following factors:

- The experiment begins with the outdoor temperature as the initial state. Both the solar wall module setups and the climate chamber are cooled to the same initial state before the start of the experiment.
- During both the heating and cooling phases, the outdoor temperature is kept constant, set to the average temperature of a typical day in that season.
- The duration of daylight and the intensity of solar radiation are also taken into consideration.

To obtain the average values of parameters such as daylight duration, solar irradiance, and outdoor temperature for a typical day in each season, data from the local meteorological station were analyzed.

The complete testing cycle lasts for 72 h, and all the experimental conditions are summarized in Table 3.

Table 3. Conditions for the steady-state experiment.

Season	Condition	Value
Spring	Daylight (solar simulation) duration	12 h
	Irradiance intensity	690 W/m^2
	Outdoor temperature	7 °C
Summer	Daylight (solar simulation) duration	12 h
	Irradiance intensity	750 W/m^2
	Outdoor temperature	19 °C
Autumn	Daylight (solar simulation) duration	10 h
	Irradiance intensity	440 W/m^2
	Outdoor temperature	10 °C
Winter	Daylight (solar simulation) duration	9 h
	Irradiance intensity	230 W/m^2
	Outdoor temperature	0 °C

In the second experiment, all test conditions were kept the same as in the first experiment, except for the solar irradiance intensity. To simulate dynamic environmental conditions, the solar simulator was turned on and off every 30 min during all the season test rounds that occurred during daylight hours.

Throughout the test, measurements were recorded every minute using the CR1000 Campbell Scientific multipurpose data logger. Solar radiation was measured using a Kipp & Zonen CMP3 pyranometer, while Type T thermocouples were used to measure temperature in both the indoor space and the phase change material (PCM). The specifications for the measuring equipment are listed in Table 4.

Table 4. Specifications of CMP, Kipp & Zonen pyranometer [38] and Type K thermocouples [39].

Equipment	Characteristics	Value
CMP, Kipp & Zonen pyranometer	Response time	20 s
	Directional response (up to 80° with 1000 W/m^2 beam)	<20 W/m^2
	Temperature dependence of sensitivity (−10 °C to +40 °C)	<4%
	Operational temperature range	−40 °C to +80 °C
	Maximum solar irradiance	2000 W/m^2
	Field of view	180°
Type K thermocouples	Temperature range	−270 °C to 1260 °C
	Accuracy	±2.2 °C or ±0.75%

2.5. Numerical Modeling of the System

The ANSYS Fluent software (2023 R1 version) was utilized for numerical modeling purposes, whereby the governing equations for fluid flow simulations were employed to conduct the simulations. One such fundamental principle of fluid dynamics is the continuity equation, which can be expressed as follows [40]:

$$\mathrm{div}(\rho V) + \partial\rho/\partial t = 0, \quad (1)$$

where div represents the divergence operator, ρ is the density of the fluid, V is the velocity vector of the fluid, and t is time.

The following assumptions were considered in the numerical modeling:

- Melting is a two-dimensional transient phenomenon.
- The movement of the PCM in its liquid state is turbulent, non-Newtonian, and incompressible.
- Viscosity, density, and thermal conductivity are constant.
- Heat generation, volume expansion, and viscous heating are not considered.

The total enthalpy of the PCM is calculated by adding the sensible enthalpy, represented by h, to the latent heat, denoted as ΔH [41]:

$$H = h + \Delta H, \quad (2)$$

and

$$h = h_{ref} + \int_{T_{ref}}^{T} C_p dT, \quad (3)$$

where h_{ref} is reference enthalpy, T_{ref} is reference temperature, and C_p is specific heat. The latent heat content is determined by taking into consideration both the latent heat of the material, denoted as L, and the liquid fraction, represented by β:

$$\Delta H = \beta L, \quad (4)$$

$$\beta = \frac{T - T_{solidus}}{T_{liquidus} - T_{solidus}}. \quad (5)$$

The amount of latent heat contained in a substance can change in direct proportion to the temperature shift between zero (for a solid) and L (for a liquid). This assumption is based on β = 0 when the material temperature is below the solidification (solidus) temperature, β = 1 when the material temperature is above the melting (liquidus) temperature, and a linear variation for temperatures between the solid and liquid states [9].

The Fusion 360 CAD tool is utilized to design a two-dimensional system drawing, which is then imported into the Design Modeler module of Ansys. This allows the drawing to be prepared for simulation in Fluent. Figure 8 displays the fluids utilized in the simulation as well as the boundary conditions that were applied.

In order to accurately replicate the conditions and dimensions of the real system, the simulation model includes an air gap (which allows space for the PCM to expand during laboratory experiments) and a plastic cover for the glass container. To determine the value of solar heat gain on each of the outer surfaces (plywood and glass), the solar heat gain coefficient (SHGC) has to be considered. Solar heat gain (SHG) can be calculated as follows:

$$SHG = SHGC \times SI, \quad (6)$$

where SI is the value of direct solar irradiation.

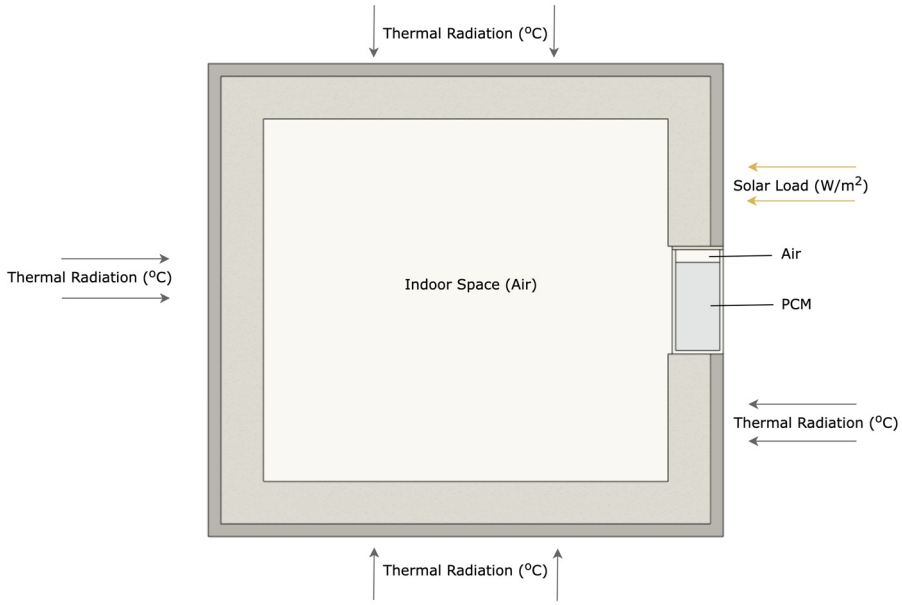

Figure 8. Design of the 2D simulation model.

To simulate isotropic turbulent flow, the k-epsilon model is utilized. The momentum equation's convective terms are discretized with a second-order upwind interpolation scheme, while the energy equation's convective terms are discretized using a first-order upwind interpolation scheme. To couple pressure and velocity, the Coupled algorithm is used, and for pressure interpolation, the PRESTO model is adopted.

3. Results

3.1. Steady-State Experiment

Figure 9 illustrates the results of a steady-state experiment conducted in a previous study [42] by our team of researchers. A series of experiments were performed to compare the behavior of two distinct PCMs during four different seasons, using the testing conditions outlined in Section 2.3.

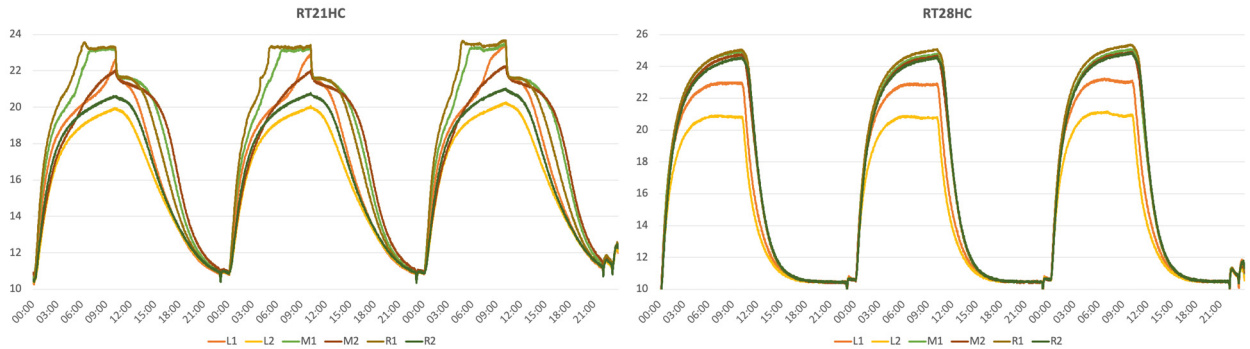

(**a**) (**b**)

Figure 9. PCM temperatures in different layers of (**a**) RT21HC and (**b**) RT28HC in the autumn conditions.

Figure 9a shows that the upper layers of RT21HC have achieved the melting temperature, resulting in the storage of latent heat, while the lower sections have yet to reach the melting point. By contrast, Figure 9b displays temperature fluctuations across various layers of RT28HC under autumn conditions, with neither layer reaching the melting temperature. Previous study findings revealed that in the autumn setup, RT28HC PCM exhibits a higher peak temperature compared to RT21HC PCM during the charging phase, but RT21HC PCM achieves a higher indoor peak temperature due to latent heat storage. Both

PCMs return to their initial outdoor temperature at the end of each daily cycle. In the spring setup, both PCMs partially melt, but RT28HC PCM reaches a higher peak temperature than RT21HC PCM. RT21HC PCM has a lower temperature during the charging phase but higher during the discharging phase. In the winter setup, neither PCM reaches its melting temperature, resulting in smaller temperature differences between the indoor space and the PCM. RT21HC PCM experiences higher average temperatures and achieves a higher room temperature compared to RT28HC PCM. In the summer setup, RT28HC PCM has a longer plateau period during the solidification phase compared to other seasons, and RT21HC PCM exhibits higher temperatures during the charging phase, but RT28HC PCM has higher temperatures during the discharging phase.

The steady-state experiments show that the behavior of the two PCMs varies depending on the season and the specific conditions of the experiment. While RT28HC reaches higher peak temperatures during the charging phase, RT21HC achieves a higher indoor peak temperature due to latent heat storage.

3.2. Dynamic Experiment

The dynamic experiment involved the implementation of the experiment plan conditions with alternating on and off solar simulation cycles.

Although each seasonal setup was tested for 72 h, no substantial variations were observed in the temperature curves when comparing them day to day. Therefore, the dynamic experimental outcomes will be evaluated based on the 24 h cycle. Figure 10a illustrates the average temperature curves of both PCMs under spring testing conditions.

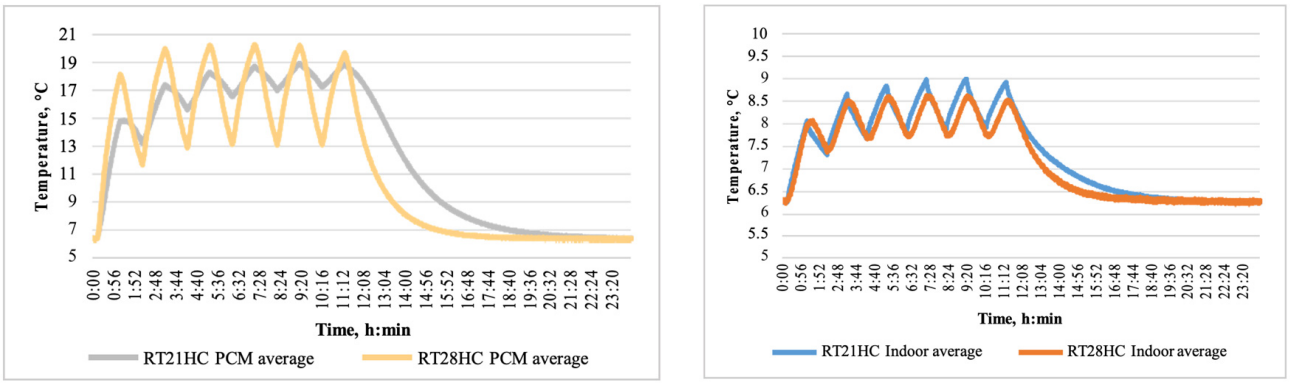

(**a**) (**b**)

Figure 10. Average temperatures in (**a**) PCMs and (**b**) indoor space; 72 h cycle. Dynamic test: Spring.

By contrast, RT28HC reaches higher temperature peaks during the daylight cycle but experiences a more significant temperature drop while the solar simulator is off, with thermal energy not being stored in the PCM due to sensible heat transition. The average indoor temperature in the RT21HC test box is higher than that in RT28HC, with a less steep slope of the temperature curve during the discharging phase (refer to Figure 10b).

Figure 11 displays temperature graphs for different layers of both PCMs. It is evident that all layers of RT21HC are in the melting phase, resulting in the storage of latent heat energy. By contrast, none of the layers of RT28HC have reached the melting point, with temperature oscillating between the highest and lowest values during the charging phase.

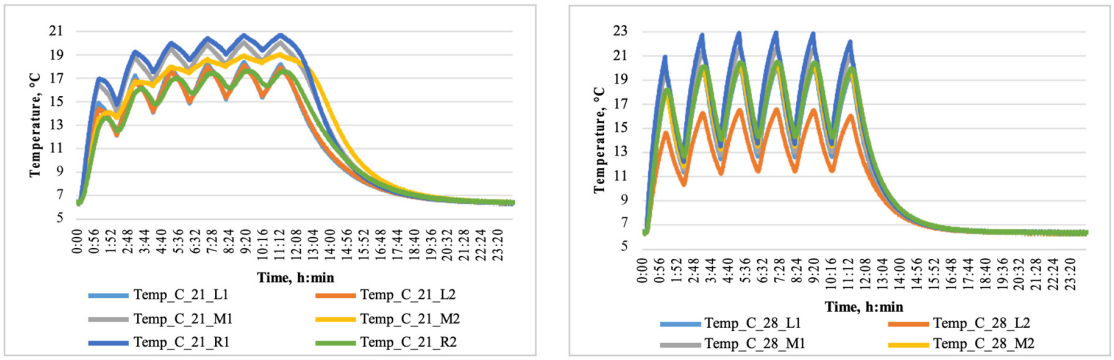

(**a**) (**b**)

Figure 11. PCM temperatures in different layers of (**a**) RT21HC and (**b**) RT28HC; 72 h cycle.

Similar temperature trends can be observed in both test stands during the autumn setup. In the summer setup, the average temperatures in both PCMs reach the melting point, with a gradual increase in temperature values (refer to Figure 12a). Although the RT21HC test box has the highest indoor temperature values, the temperature peaks do not exceed 21 °C (refer to Figure 12b). Upon observing temperatures in different locations of RT21HC (refer to Figure 13a), it is evident that all layers of the PCM have exceeded the melting temperature, and the PCM is completely melted starting from around 2:00, resulting in sensible heat energy storage. In the case of RT28HC (refer to Figure 13b), only one spot in the upper layer (L2) has not reached the melting point, indicating partial liquefaction of the PCM and partial latent heat energy storage. However, at the end of the 24 h cycle, the temperature in RT21HC PCM is 2–3 °C higher than in RT28HC, depending on the location of the layer measurement.

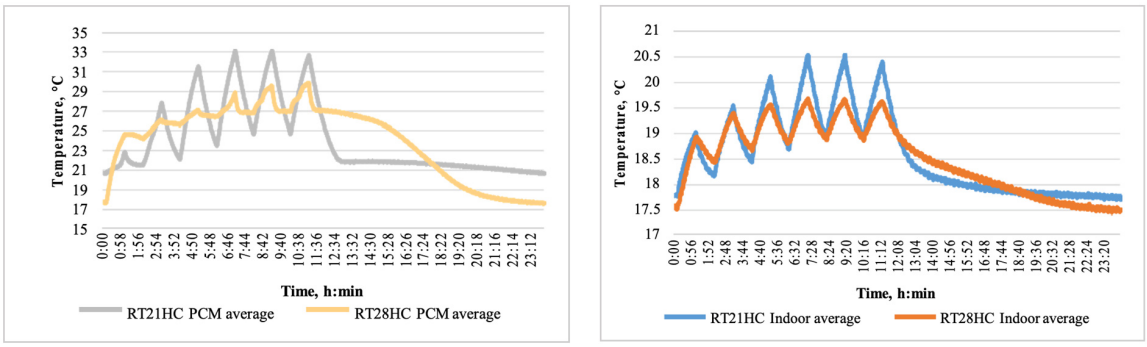

(**a**) (**b**)

Figure 12. Average temperatures in (**a**) PCMs and (**b**) indoor space; 72 h cycle. Dynamic test: summer.

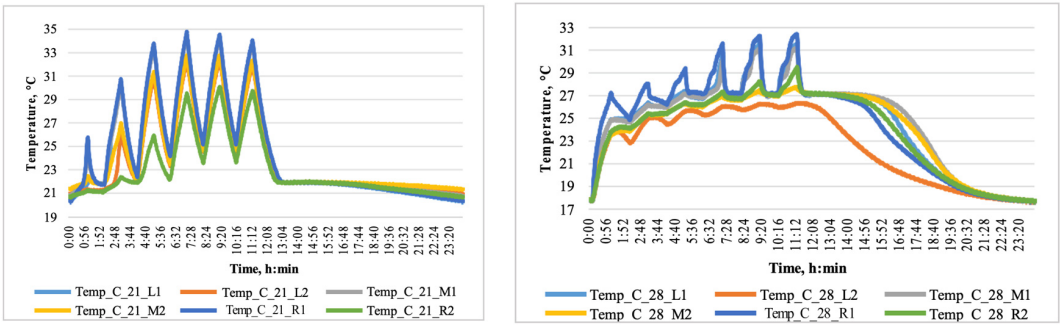

(**a**) (**b**)

Figure 13. PCM temperatures in different layers of (**a**) RT21HC and (**b**) RT28HC; 72 h cycle. Dynamic test: summer.

Figure 14 presents a comparison of the highest average temperatures in both PCMs and indoor spaces between the steady-state and dynamic experiments. Although there are similar temperature trends in both types of experiments, the overall temperature values are higher in the steady-state tests due to the absence of solar irradiance dropouts. While RT28HC reaches higher PCM peak temperatures in autumn, winter, and spring, RT21HC exhibits the highest indoor space temperatures in all seasons. This suggests that RT21HC is more effective in storing thermal energy in the PCM and releasing it into the indoor compartment.

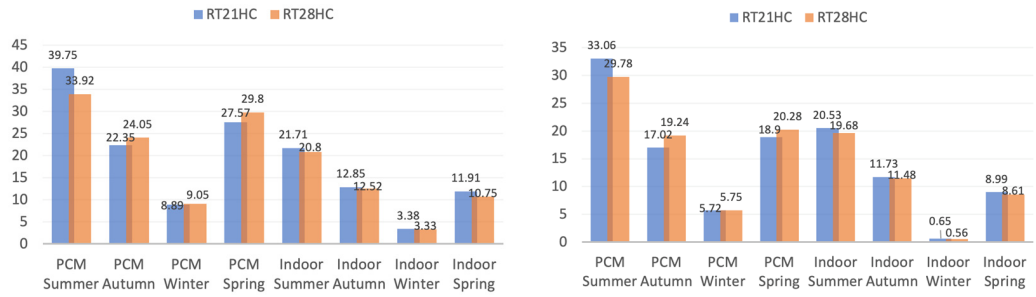

(**a**) (**b**)

Figure 14. Comparison between the highest temperatures reached by RT21HC and RT28HC in (**a**) steady-state test and (**b**) dynamic test.

3.3. Numerical Simulation

To assess how the system would perform under varying climate conditions such as changes in solar irradiance and outside temperature, it is essential to verify the accuracy of the model against experimental data. To accomplish this, a laboratory test was carried out where both experimental setups were heated until the PCM completely melted, and subsequently cooled to the ambient temperature. The results of the experimental test, as well as simulated temperature curves, are represented in Figure 15. Since the laboratory test was conducted inside a climate chamber that maintains a consistent temperature through its cooling system, the numerical calculations must consider the airflow velocity to match the dynamics of the actual system, which was recorded at approximately 0.5 m/s.

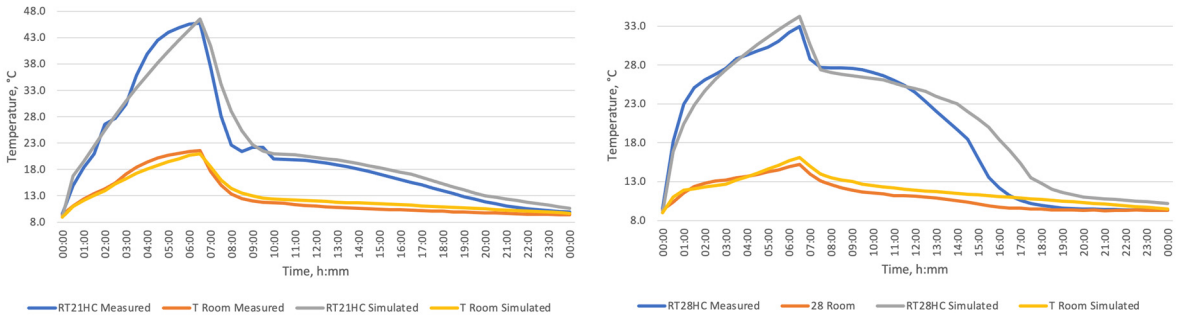

(**a**) (**b**)

Figure 15. Comparison between simulated and experimentally collected data of (**a**) RT21HC and (**b**) RT28HC PCMs.

To conduct the numerical simulation, information on the outside temperature and solar irradiance was gathered from two cities located in different regions of Europe. Helsinki, Finland, in the north, and Seville, Spain, in the south, were chosen for this purpose. The National Solar Radiation Database was used to collect data from the past three years. Hourly averages of the direct solar radiation and outside temperature were calculated for each of the four seasons—spring, summer, autumn, and winter.

The numerical model relies on various conditions and assumptions, including the use of global horizontal solar irradiance for solar load calculations, an assumption of clear skies, and the consideration that only the front-facing side of the box is impacted by the solar load; the wind direction and speed are ignored in these calculations. Ten simulations were conducted using the developed model, with six of them simulating the environmental conditions of spring, summer, and autumn in Helsinki, while the remaining four simulations imitated spring and winter conditions in Seville. The decision not to perform simulations for wintertime in Helsinki and summertime in Seville was based on previous laboratory experiments which indicated that neither of the PCMs provided any advantages in extremely hot or cold conditions.

The climate in Helsinki during spring and autumn is comparable and mild, with the exception of slightly higher outdoor temperatures in autumn. Figure 16 represents simulation results from the spring test in Helsinki.

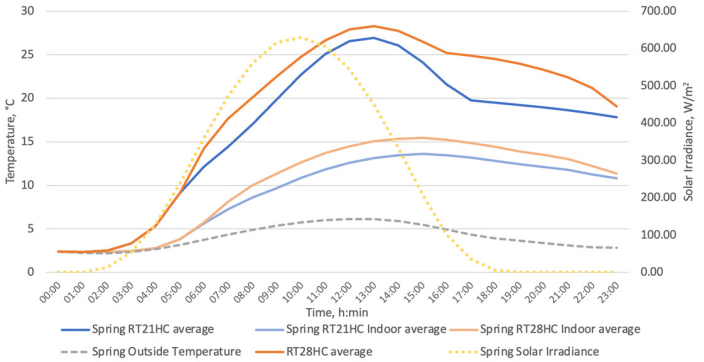

Figure 16. Average temperature in the PCMs and indoor room. Simulation results: Helsinki—spring.

From the Helsinki—spring graphs, it is evident that both PCMs underwent a partial melting process and absorbed thermal energy. Further analysis revealed that the RT28HC PCM experienced a slightly higher average temperature compared to the RT21HC examined. However, at the end of the 24 h cycle, both PCMs attained almost identical temperature values. The ambient temperature outside did not exceed 6 °C during the testing period. This implies that all of the thermal energy absorbed by the PCMs was from solar radiation.

Figure 17 displays the outcomes of the Helsinki autumn simulation. It reveals that the maximum average temperature of RT28HC was approximately 6 °C higher than that of RT21HC. However, by the end of the 24 h cycle, the temperature of RT28HC dropped 6 °C below that of RT21HC. This result can be attributed to the fact that although RT28HC attained a higher temperature while solar radiation was present, it was unable to reach its melting point. Therefore, it lost the absorbed heat by the end of the cycle. By contrast, RT21HC was able to store enough thermal energy to maintain a higher temperature in the room by the end of the cycle.

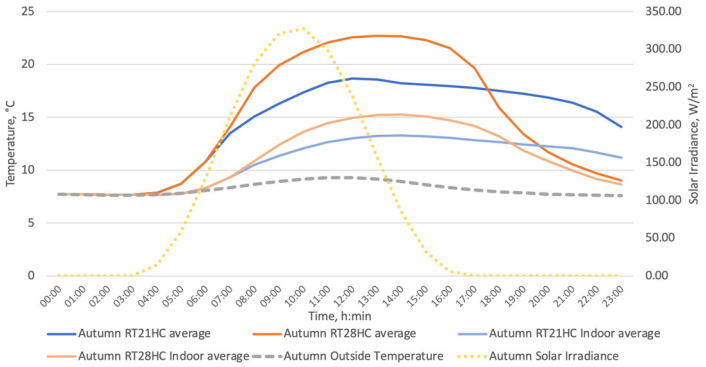

Figure 17. Average temperature in the PCMs and indoor room. Simulation results: Helsinki—autumn.

Compared to other European cities, especially those in Southern Europe, Helsinki experiences cooler and more moderate summers. Throughout the months of June, July, and August, the average high temperature in Helsinki typically falls between 18 °C to 22 °C, while the average low temperature ranges from 10 °C to 14 °C. Figure 18 illustrates the temperature graphs of the summer season in Helsinki. As solar radiation reaches high levels, both PCMs melted. However, it is evident that RT28HC had the advantage of a higher melting point temperature, preventing the room from overheating. In these conditions, RT28HC exhibited smoother temperature fluctuations throughout the entire cycle, which resulted in a more comfortable environment in the room.

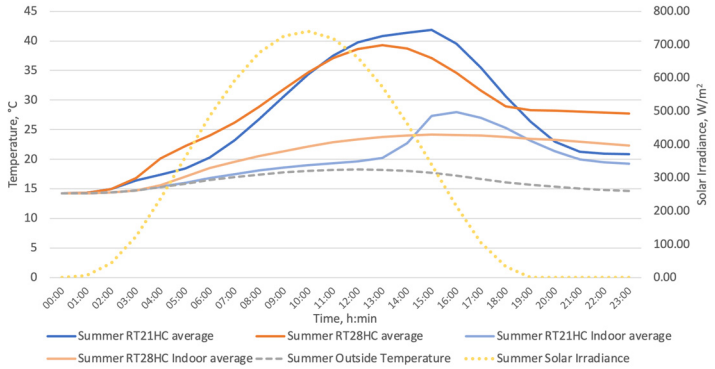

Figure 18. Average temperature in the PCMs and indoor room. Simulation results: Helsinki—summer.

Compared to Northern Europe, Southern Europe, exemplified by Seville, receives a higher amount of sunlight throughout the year in all seasons. Seville experiences an average of 129 sunny days annually, and the solar intensity is higher than in other European cities. In spring, the solar irradiance value can surpass 900 W/m^2, which raises concerns about the possibility of overheating. However, the nighttime temperatures are still relatively low, not exceeding 12 °C, which may require additional heating. The simulation results of Seville in spring are depicted in Figure 19. It is evident that RT21HC overheats in such a climate, causing the room temperature to rise to nearly 35 °C. Conversely, RT28HC has a great potential to prevent the room from overheating during the daytime while ensuring comfortable temperatures at night, without requiring additional heating. This case underscores the advantage of RT28HC's higher heat storage capacity, allowing it to absorb more thermal energy than RT21HC.

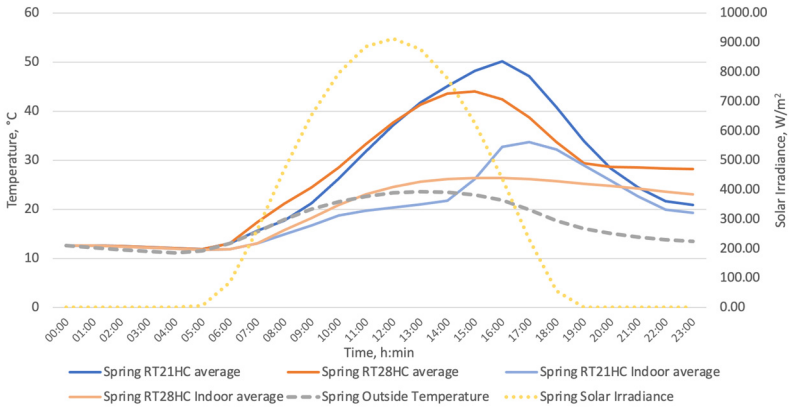

Figure 19. Average temperature in the PCMs and indoor room. Simulation results: Seville—spring.

Seville has a milder winter compared to many other European cities due to its southern location and Mediterranean climate. The average temperature in Seville during the winter months (December to February) ranges from 8 °C to 18 °C, which is considerably warmer than many other European cities during the same period. Yet, additional heating

is necessary for most of the time. The average PCM temperatures in the Seville—winter numerical simulation are illustrated in Figure 20.

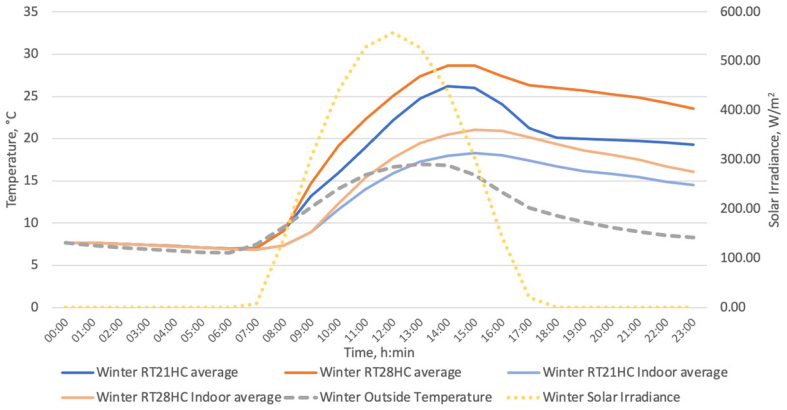

Figure 20. Average temperature in the PCMs and indoor room. Simulation results: Seville—winter.

Both PCMs exhibit comparable behavior in this scenario, as they have both achieved the melting point temperature and stored thermal energy through latent heat. The indoor temperature profiles follow a similar pattern, but the RT28HC performs slightly better, as it is able to attain a higher maximum room temperature of approximately 21 °C. Figure 21 represents the comparison of the highest liquid fraction reached in the PCMs in every simulation. It is clearly seen that RT21HC has melted fully in two cases, Helsinki—summer and Seville—spring, which highlights the potential for overheating. In all of the cases, RT21HC has reached liquid fraction values due to its lower heat storage capacity compared to RT28HC.

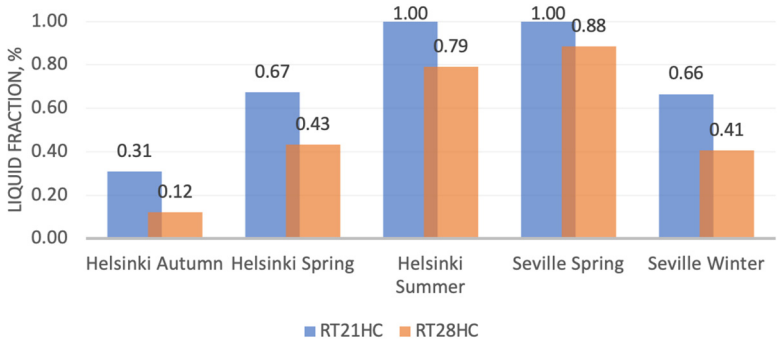

Figure 21. Comparison of the highest reached melted fraction of the PCMs in all simulations.

4. Discussion and Conclusions

Experimental and numerical research was conducted to compare two different phase change materials (PCMs) with melting temperatures of 21 °C and 28 °C, respectively, under specific climatic conditions that mimic the four seasons of the year. A small-scale model of a building was utilized for the experiment, comprising a test box with a thermal envelope and an indoor area subjected to heating and cooling loads within a climate chamber. Two types of experiments, steady-state and dynamic, were performed, and two parameters were compared: the average temperature of the PCM and the average temperature of the indoor space in the test box. The results showed that RT21HC PCM had a higher average indoor temperature than RT28HC, with a less steep slope of the temperature curve during the discharging phase. By contrast, RT28HC had higher temperature peaks during the daylight cycle but experienced a more significant temperature drop while the solar simulator was off, with thermal energy not being stored in the PCM due to sensible heat transition. The results also showed that all layers of RT21HC were in the melting phase, resulting in the storage of latent heat energy, while none of the layers of RT28HC reached the melting point,

with temperature oscillating between the highest and lowest values during the charging phase. In the summer setup, both PCMs reached the melting point, with a gradual increase in temperature values. The experimental results suggest that RT21HC is more effective in storing thermal energy in the PCM and releasing it into the indoor compartment compared to RT28HC in particular climate conditions.

The numerical modeling gives an insight into the effectiveness of each of the tested phase change materials applied in different climate zones. The laboratory test was carried out to verify the accuracy of the model against experimental data. The numerical simulations were conducted using the information on outside temperature and solar irradiance gathered from two cities in different regions of Europe—Helsinki, Finland, and Seville, Spain. The simulation results showed that the PCMs underwent a partial melting process and absorbed thermal energy during the spring, autumn, and summer seasons in Helsinki. The RT28HC PCM experienced a slightly higher average temperature compared to RT21HC examined in Helsinki. However, at the end of the 24 h cycle, both PCMs attained almost identical temperature values. By contrast, during the autumn season in Helsinki, the maximum average temperature of RT28HC was approximately 6 °C higher than that of RT21HC. However, by the end of the 24 h cycle, the temperature of RT28HC dropped 6 °C below that of RT21HC. The summer season simulations in Helsinki showed that both PCMs melted, but RT28HC had the advantage of a higher melting point temperature, preventing the room from overheating. In Seville, the RT28HC PCM had the potential to prevent the room from overheating during the daytime, while ensuring comfortable temperatures at night, without requiring additional heating. In the winter season in Seville, both PCMs achieved the melting point temperature and stored thermal energy through latent heat, but RT28HC performed slightly better.

This study provides data on thermodynamic processes under various outdoor temperatures and solar simulation intensities, which can be used to validate mathematical models and explore different design scenarios for PCM-enriched building components at various scales, from small-scale models to real-size buildings. This research is part of a larger effort to develop PCM-enriched adaptive solar facade systems that can actively contribute to building energy balance and represent a novel solution in the field of building components.

Author Contributions: Conceptualization, A.B.; Methodology, J.N.; Software, J.N.; Data curation, R.F. and Z.Z.; Writing—original draft, R.V.; Writing—review & editing, R.V. and J.N.; Visualization, J.N.; Supervision, R.V. All authors have read and agreed to the published version of the manuscript.

Funding: This work was supported by the European Social Fund within Project No. 8.2.2.0/20/I/008 «Strengthening of Ph.D. students and academic personnel of Riga Technical University and BA School of Business and Finance in the strategic fields of specialization» of the Specific Objective 8.2.2 «To Strengthen Academic Staff of Higher Education Institutions in Strategic Specialization Areas» of the Operational Program «Growth and Employment».

Data Availability Statement: Not applicable.

Conflicts of Interest: The authors declare no conflict of interest.

References

1. European Commission. *The European Green Deal*; European Commission: Brussels, Belgium, 2019.
2. European Union. Directive (EU) 2018/844 of the European Parliament and of the Council of 30 May 2018 amending Directive 2010/31/EU on the energy performance of buildings and Directive 2012/27/EU on energy efficiency. *Off. J. Eur. Union* **2018**, *L156*, 75.
3. EU. Directive (EU) 2018/2001 of the European Parliament and of the Council on the promotion of the use of energy from renewable sources. *Off. J. Eur. Union* **2018**, *L328*, 82–209.
4. Ahangari, M.; Maerefat, M. An innovative PCM system for thermal comfort improvement and energy demand reduction in building under different climate conditions. *Sustain. Cities Soc.* **2019**, *44*, 120–129. [CrossRef]
5. Saffari, M.; Roe, C.; Finn, D.P. Improving the building energy flexibility using PCM-enhanced envelopes. *Appl. Therm. Eng.* **2022**, *217*, 119092. [CrossRef]
6. Alshuraiaan, B. Efficient Utilization of Pcm in Building Envelope in a Hot Environment Condition. *SSRN Electron. J.* **2022**, *16*, 100205. [CrossRef]

7. Arumugam, P.; Ramalingam, V.; Vellaichamy, P. Effective PCM, insulation, natural and/or night ventilation techniques to enhance the thermal performance of buildings located in various climates—A review. *Energy Build.* **2022**, *258*, 111840. [CrossRef]
8. Al-Saadi, S.N.; Zhai, Z. Modeling phase change materials embedded in building enclosure: A review. *Renew. Sustain. Energy Rev.* **2013**, *21*, 659–673. [CrossRef]
9. Ručevskis, S.; Akishin, P.; Korjakins, A. Performance Evaluation of an Active PCM Thermal Energy Storage System for Space Cooling in Residential Buildings. *Environ. Clim. Technol.* **2019**, *23*, 74–89. [CrossRef]
10. Yassi, M.E.; Abbassi, I.E.; Pierre, A.; Melinge, Y. Comparative Study of Two Materials Combining a Standard Building Material with a PCM. *Fluid Dyn. Mater. Process.* **2023**, *19*, 1283–1290. [CrossRef]
11. Rehman, A.U.; Sheikh, S.R.; Kausar, Z.; Mccormack, S.J. Numerical Simulation of a Novel Dual Layered Phase Change Material Brick Wall for Human Comfort in Hot and Cold Climatic Conditions. *Energies* **2021**, *14*, 4032. [CrossRef]
12. Rucevskis, S.; Akishin, P.; Korjakins, A. Parametric analysis and design optimisation of PCM thermal energy storage system for space cooling of buildings. *Energy Build.* **2020**, *224*, 110288. [CrossRef]
13. Selvaraju, A.P.; Ranganathan, A.; Vincent, A.A.R.; Arumugam, P.; Ramalingam, V. Thermal management analysis of PCM integration in building using a novel performance parameter PCM effectiveness Index. *Therm. Sci.* **2022**, *26*, 883–895. [CrossRef]
14. Teja, P.N.S.; Gugulothu, S.K.; Sastry, G.R.; Burra, B.; Bhurat, S.S. Numerical analysis of nanomaterial-based sustainable latent heat thermal energy storage system by improving thermal characteristics of phase change material. *Environ. Sci. Pollut. Res.* **2022**, *29*, 50937–50950. [CrossRef] [PubMed]
15. Liang, D.M.; Ibrahim, M.; Saeed, T.; El-Refaey, A.M.; Li, Z.X.; Fagiry, M.A. Simulation of a Trombe wall with a number of semicircular fins placed on the absorber plate for heating a room in the presence of nano-PCM. *J. Build. Eng.* **2022**, *50*, 104173. [CrossRef]
16. Su, W.G.; Darkwa, J.; Kokogiannakis, G. Numerical thermal evaluation of laminated binary microencapsulated phase change material drywall systems. *Build. Simul.* **2020**, *13*, 89–98. [CrossRef]
17. Al-Mudhafar, A.H.N.; Hamzah, M.T.; Tarish, A.L. Potential of integrating PCMs in residential building envelope to reduce cooling energy consumption. *Case Stud. Therm. Eng.* **2021**, *27*, 101360. [CrossRef]
18. Sarbu, I.; Sebarchievici, C. A comprehensive review of thermal energy storage. *Sustainability* **2018**, *10*, 191. [CrossRef]
19. Allison, T.; Smith, N.R.; Ma, Z. Chapter 1—Introduction to energy storage. In *Thermal, Mechanical, and Hybrid Chemical Energy Storage Systems*; Brun, K., Allison, T., Dennis, R.B.T., Eds.; Academic Press: Cambridge, MA, USA, 2021; pp. 1–25. ISBN 978-0-12-819892-6. Available online: https://www.sciencedirect.com/science/article/pii/B9780128198926000010 (accessed on 12 February 2023).
20. Ahmed, N.; Elfeky, K.E.; Lu, L.; Wang, Q.W. Thermal and economic evaluation of thermocline combined sensible-latent heat thermal energy storage system for medium temperature applications. *Energy Convers. Manag.* **2019**, *189*, 14–23. [CrossRef]
21. IRENA. *Innovation Outlook Thermal Energy Storage*; IRENA: Masdar City, United Arab Emirates, 2020.
22. Al-Yasiri, Q.; Szabó, M. Paraffin as a Phase Change Material to Improve Building Performance: An Overview of Applications and Thermal Conductivity Enhancement Techniques. *Renew. Energy Environ. Sustain.* **2021**, *6*, 38. [CrossRef]
23. Ansu, A.K.; Sharma, R.K.; Tyagi, V.V.; Sari, A.; Ganesan, P.; Tripathi, D. A cycling study for reliability, chemical stability and thermal durability of polyethylene glycols of molecular weight 2000 and 10,000 as organic latent heat thermal energy storage materials. *Int. J. Energy Res.* **2020**, *44*, 2183–2195. [CrossRef]
24. Duttaluru, G.; Singh, P.; Kumar, A. Methods to enhance the thermal properties of organic phase change materials: A review. *Mater. Today Proc.* **2022**, *63*, 685–691. [CrossRef]
25. Heier, J.; Bales, C.; Martin, V. Combining thermal energy storage with buildings—A review. *Renew. Sustain. Energy Rev.* **2015**, *42*, 1305–1325. [CrossRef]
26. Soibam, J. Numerical Investigation of a Heat Exchanger Using Phase Change Materials (PCMs). Master's Thesis, Mälardalen University, Västerås, Sweden, 2017.
27. Ben Romdhane, S.; Amamou, A.; Ben Khalifa, R.; Saïd, N.M.; Younsi, Z.; Jemni, A. A review on thermal energy storage using phase change materials in passive building applications. *J. Build. Eng.* **2020**, *32*, 101563. [CrossRef]
28. Lai, C.M.; Hokoi, S. Thermal performance of an aluminum honeycomb wallboard incorporating microencapsulated PCM. *Energy Build.* **2014**, *73*, 37–47. [CrossRef]
29. Silva, T.; Vicente, R.; Soares, N.; Ferreira, V. Experimental testing and numerical modelling of masonry wall solution with PCM incorporation: A passive construction solution. *Energy Build.* **2012**, *49*, 235–245. [CrossRef]
30. De Gracia, A.; Navarro, L.; Castell, A.; Ruiz-Pardo, Á.; Alvárez, S.; Cabeza, L.F. Experimental study of a ventilated facade with PCM during winter period. *Energy Build.* **2013**, *58*, 324–332. [CrossRef]
31. Rubitherm. PCM RT-LINE. Available online: https://www.rubitherm.eu/en/productcategory/organische-pcm-rt (accessed on 20 April 2023).
32. Norlén, U. Estimating thermal parameters of outdoor test cells. *Build. Environ.* **1990**, *25*, 17–24. [CrossRef]
33. Madsen, H.; Holst, J. Estimation of continuous-time models for the heat dynamics of a building. *Energy Build.* **1995**, *22*, 67–79. [CrossRef]
34. Wouters, P.; Vandaele, L.; Voit, P.; Fisch, N. The use of outdoor test cells for thermal and solar building research within the PASSYS project. *Build. Environ.* **1993**, *28*, 107–113. [CrossRef]

35. Guo, J.; Zhang, G. Investigating the performance of the PCM-integrated building envelope on a seasonal basis. *J. Taiwan Inst. Chem. Eng.* **2021**, *124*, 91–97. [CrossRef]
36. Wald, N.J.; Rodeck, C.; Hackshaw, A.K.; Walters, J.; Chitty, L.; Mackinson, A.M. Solar Energy Perspectives: Executive summary. *J. Med. Screen.* **2003**, *10*, 56–57. [CrossRef]
37. Cho, Y.; Kim, J.J. Lifetime decrease of halogen lamps for automotive by duty cycle stress. *IEEE Trans. Reliab.* **2011**, *60*, 550–556. [CrossRef]
38. OTT Hydromet GMBH. Pyranometer CMP3 | SMP3. Available online: https://www.otthydromet.com/en/p-kippzonen-smp3-pyranometer/0374900 (accessed on 12 February 2023).
39. Thermocouple. Type K Thermocouple. Available online: https://www.thermocoupleinfo.com/type-k-thermocouple.htm (accessed on 12 February 2023).
40. ANSYS. Knowledge Creation Diffusion Utilization. In *ANSYS Fluent User' s Guide*; Release 13.0.; ANSYS, Inc.: Canonsburg, PA, USA, 2013; Volume 15317, pp. 724–746.
41. Hassab, M.A.; Sorour, M.M.; Mansour, M.K.; Zaytoun, M.M. Effect of volume expansion on the melting process's thermal behavior. *Appl. Therm. Eng.* **2017**, *115*, 350–362. [CrossRef]
42. Vanaga, R.; Narbuts, J.; Freimanis, R.; Blumberga, A. Laboratory Testing of Different Melting Temperature Phase Change Materials Under Four Season Conditions for Thermal Energy Storage in Building Envelope. In Proceedings of the International Conference on Applied Energy, Virtual, 29 November–5 December 2021.